UC Berkeley
UC Berkeley Previously Published Works

Title
Evaluation of the Stability of Diamine-Appended Mg2(dobpdc) Frameworks to Sulfur Dioxide

Authors
Parker, Surya T
Smith, Alex
Forse, Alexander C
et al.

J|A|C|S

JOURNAL OF THE AMERICAN CHEMICAL SOCIETY

Article

Evaluation of the Stability of Diamine-Appended Mg₂(dobpdc) Frameworks to Sulfur Dioxide

Surya T. Parker, Alex Smith, Alexander C. Forse, Wei-Chih Liao, Florian Brown-Altvater, Rebecca L. Siegelman, Eugene J. Kim, Nicholas A. Zill, Wenjun Zhang, Jeffrey B. Neaton, Jeffrey A. Reimer, and Jeffrey R. Long*

Cite This: https://doi.org/10.1021/jacs.2c07498

Read Online

ACCESS | 📊 Metrics & More | 📑 Article Recommendations | 🆘 Supporting Information

ABSTRACT: Diamine-appended Mg₂(dobpdc) (dobpdc⁴⁻ = 4,4′-dioxidobiphenyl-3,3′-dicarboxylate) metal−organic frameworks are a promising class of CO_2 adsorbents, although their stability to SO_2—a trace component of industrially relevant exhaust streams—remains largely untested. Here, we investigate the impact of SO_2 on the stability and CO_2 capture performance of dmpn−Mg₂(dobpdc) (dmpn = 2,2-dimethyl-1,3-propanediamine), a candidate material for carbon capture from coal flue gas. Using SO_2 breakthrough experiments and CO_2 isobar measurements, we find that the material retains 91% of its CO_2 capacity after saturation with a wet simulated flue gas containing representative levels of CO_2 and SO_2, highlighting the robustness of this framework to SO_2 under realistic CO_2 capture conditions. Initial SO_2 cycling experiments suggest dmpn−Mg₂(dobpdc) may achieve a stable operating capacity in the presence of SO_2 after initial passivation. Evaluation of several other diamine−Mg₂(dobpdc) variants reveals that those with *primary,primary* (1°,1°) diamines, including dmpn−Mg₂(dobpdc), are more robust to humid SO_2 than those featuring *primary,secondary* (1°,2°) or *primary,tertiary* (1°,3°) diamines. Based on the solid-state ¹⁵N NMR spectra and density functional theory calculations, we find that under humid conditions, SO_2 reacts with the metal-bound primary amine in 1°,2° and 1°,3° diamine-appended Mg₂(dobpdc) to form a metal-bound bisulfite species that is charge balanced by a primary ammonium cation, thereby facilitating material degradation. In contrast, humid SO_2 reacts with the free end of 1°,1° diamines to form ammonium bisulfite, leaving the metal−diamine bond intact. This structure−property relationship can be used to guide further optimization of these materials for CO_2 capture applications.
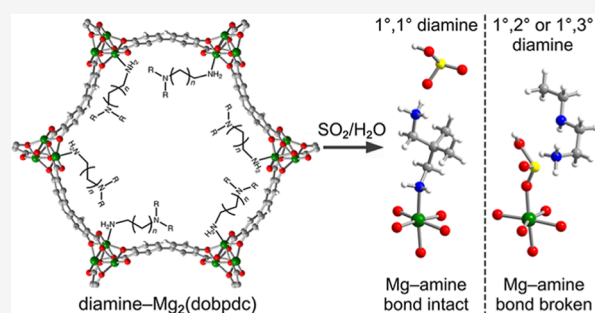
■ INTRODUCTION

Carbon dioxide emissions derived from fossil fuel combustion have been steadily rising over the last several decades and are widely acknowledged to be the leading cause of global climate change.[1] In tandem with increasing reliance on low- and zero-carbon energy technologies, restricting global warming to <2 °C above preindustrial levels will require a targeted reduction in anthropogenic CO_2 emissions within the current energy infrastructure. Coal-fired power plants account for approximately 30% of CO_2 emissions worldwide,[1,2] and, as fossil fuels, are projected to continue supplying the majority of global energy in the short term. Post combustion capture from these point sources stands as a critical mitigation strategy.[3] Aqueous amine solutions represent the most mature carbon capture technology, although their wide-spread implementation has been stymied due to their intrinsically high regeneration energies, low CO_2 capacities, and operational issues related to their corrosivity and volatility.[3,4]

In recent years, amine-functionalized solid adsorbents—including porous carbons, silicas, and metal−organic frameworks (MOFs)—have gained increasing attention as promising alternatives for energy-efficient carbon capture, owing to their potentially low regeneration energy, selectivity for CO_2 at low concentrations relevant to flue streams, and cycling stability.[5−14] Among these materials, MOFs of the type diamine−Mg₂(dobpdc) (dobpdc⁴⁻ = 4,4′-dioxidobiphenyl-3,3′-dicarboxylate)—and recently tetraamine−Mg₂(dobpdc)[15]—have attracted significant interest, given their high adsorption capacities, selectivities for CO_2 over N_2, and stability in the presence of water.[16−23] These materials reversibly adsorb CO_2 via a cooperative mechanism involving CO_2 insertion into the framework metal−amine bonds to form chains of ammonium carbamate that propagate down the framework channels. As a result of this unique behavior, CO_2 uptake occurs in a stepwise fashion, such that initial adsorption and subsequent

A

saturation occur within a narrow pressure or temperature range. These adsorbents can therefore achieve very high CO_2 working capacities with relatively small temperature or pressure swings compared to typical Langmuir-type adsorbents, which represent the vast majority of other amine-functionalized materials known to date.

Importantly, the characteristic CO_2 adsorption threshold of diamine−Mg_2(dobpdc) can be tuned by changing the appended amine, allowing optimization for a specific capture application.[18−20] For example, dmpn−Mg_2(dobpdc) (dmpn = 2,2-dimethyl-1,3-propanediamine) exhibits a CO_2 adsorption step at 15 mbar and 40 °C, ideally positioned for 90% CO_2 capture from coal flue gas.[19] This material is also unusual in that it adsorbs CO_2 via a mixed mechanism to form carbamic acids and ammonium carbamate chains that propagate along the framework channels at adjacent vertices and interact through hydrogen bonding (Figure 1).[19,24] Recent modeling of
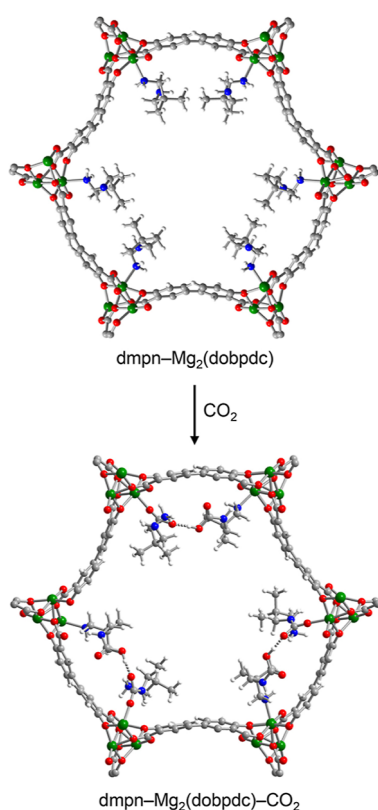
Figure 1. Structures of dmpn−Mg_2(dobpdc) before (upper) and after (lower) uptake of CO_2, generated from vdW-corrected DFT calculations, illustrating the formation of a 1:1 mixture of ammonium carbamate to carbamic acid chains.[24] Green, gray, red, blue, and white spheres represent Mg, C, O, N, and H atoms, respectively. Views are down the c axis.

the performance of dmpn−Mg_2(dobpdc) in various temperature-swing adsorption processes revealed that it may be cost-competitive with state-of-the-art monoethanolamine solutions for CO_2 capture from coal flue gas if the heat generated upon adsorption can be recycled efficiently.[25]

Further advancement of diamine-appended Mg_2(dobpdc) materials toward carbon capture applications requires the rigorous evaluation of their stabilities and properties under practical working conditions. While some of these frameworks have been shown to maintain excellent capture performance in

the presence of humidity and even O_2,[19,20,22,23,26,27] their performance in the presence of SO_2, another key component of coal flue gas, remains largely unexplored.[22,23] This is in contrast to the growing number of literature studies that have examined the stability of other solid adsorbents to SO_2, such as zeolitic imidazolate frameworks and amine-appended silicas.[28−32] Although coal flue gas is treated to remove a portion of the SO_2 to comply with environmental regulations,[8,33,34] a non-negligible concentration remains in the outlet stream. For example, based on tabulated data for CO_2 and SO_2 emissions from coal-fired power plants in the United States and assuming an average flue gas CO_2 concentration of 13.5%,[35] the flue gas streams of established plants contain an estimated SO_2 concentration of 80 ppm (see Section S2 of the Supporting Information for details).[36] Even with new regulations enacted in 2010, the flue streams of new or remodeled power plants can contain as much as 20 to 50 ppm SO_2.[37,38] Modifying current desulfurization processes to remove the residual SO_2 would increase the costs associated with an already expensive process.[33,39−43] As such, candidate CO_2 capture adsorbents must be robust and maintain their capture performance in the presence of trace quantities of SO_2,[7] particularly in the presence of water, which can constitute as much as 5 to 15% of the coal flue gas.[8,44,45] While it is a growing area of interest, few studies to date have investigated the effect of SO_2 on the performance of CO_2 capture materials and even fewer under relevant concentrations of SO_2 in the presence of humidity.

To the best of our knowledge, only two studies have reported preliminary data on the stability and CO_2 capture performance of diamine−Mg_2(dobpdc) following exposure to humid SO_2.[22,23] In brief, Mg_2(dobpdc) appended with the *primary,primary* (1°,1°) diamines ethylenediamine (en), 1-methylethylenediamine (men), and 1,1-dimethylethylenediamine (dmen) and *primary,secondary* (1°,2°) N-isopropylethylenediamine (i-2) and N-ethylethylenediamine (e-2) were exposed to 500 ppm of SO_2 with 100% humidity for periods of up to 2 h. The men-, dmen-, e-2-, and i-2-appended variants were reported to retain >90% of their CO_2 capacity under all conditions, whereas the capacity of en−Mg_2(dobpdc) diminished by more than 30% upon exposure for more than 30 min.[22,23] To rationalize the superior performance of men−, dmen−, i-2−, and e-2−Mg_2(dobpdc) relative to en−Mg_2(dobpdc), it was proposed that sterically encumbering substituents on the amines could provide enhanced stability in the presence of SO_2. However, this hypothesis was not tested further, and a meaningful analysis of the data is complicated by the fact that en−Mg_2(dobpdc) partially decomposes in the presence of water alone.[22,23,27] Additionally, complete saturation of the materials with SO_2 was not measured or confirmed. Thus, further investigation is needed to develop a detailed understanding of how SO_2 exposure impacts the performance of these materials over extended exposure times, the nature of any interaction between the framework and SO_2, and the role of the diamine structure in dictating relative stability.

Here, we present an in-depth study of the stability of dmpn−Mg_2(dobpdc) to humid SO_2 using SO_2 breakthrough experiments and CO_2 adsorption measurements. We find that the CO_2 capacity of the material decreases following exposure to humid SO_2, although this capacity loss is substantially attenuated when the sample is exposed to a simulated flue gas (30 ppm SO_2, 14% CO_2, ~2% H_2O, balance N_2 at 40 °C). Using solid-state NMR spectroscopy and van der Waals

(vdW)-corrected density functional theory (DFT), we identify that in the presence of humidity, SO_2 reacts with the free end of the appended diamine in dmpn–Mg_2(dobpdc) to form ammonium bisulfite. Analysis of several other Mg_2(dobpdc) variants appended indicates that ammonium bisulfite formation upon SO_2 exposure is a generalizable phenomenon in these materials. However, in materials featuring $1°,2°$ and $1°,3°$ diamines, SO_2 preferentially reacts with the metal-bound amine, rendering these variants far less stable to the gas than those appended with $1°,1°$ amines. These results provide unprecedented insight into the factors governing the stability of diamine-appended Mg_2(dobpdc) materials to humid SO_2 and will support their iterative design for real-world applications.

■ RESULTS AND DISCUSSION

Breakthrough Experiments. The stability of dmpn–Mg_2(dobpdc) to SO_2 was examined by carrying out SO_2 breakthrough experiments followed by analysis of the CO_2 capture performance of the material using isobar measurements. Breakthrough adsorption measurements were conducted using a custom-built instrument designed to enable exposure of the material to controlled gas mixtures containing SO_2 and the detection of SO_2 outlet concentrations over time (see Section S3 of the Supporting Information and Figure S3). An initial breakthrough experiment was carried out with a stream containing 30 ppm of dry SO_2 in a balance of N_2 at 40 °C and atmospheric pressure. Under these conditions, SO_2 breakthrough occurred within minutes, and negligible uptake was measured (Figure S5 and Table S1). A CO_2 adsorption isobar collected for dmpn–Mg_2(dobpdc) after this experiment revealed no change in the capacity of the material (Figure 2a). Furthermore, the material retained more than 90% of its CO_2 capacity after exposure to concentrations of SO_2 up to 300 ppm in N_2 (Figure S7). In all, dmpn–Mg_2(dobpdc) is among only a handful of other amine-functionalized adsorbents in the literature found to be robust to such levels of dry SO_2.[8,28−30,46−49]

We next examined the stability of dmpn–Mg_2(dobpdc) in the presence of SO_2 and humidity by carrying out a breakthrough measurement using an inlet stream containing 30 ppm of SO_2 and ~2% water in N_2 at atmospheric pressure and 40 °C. Under these conditions, SO_2 breakthrough took more than 2 days, significantly longer than under dry conditions. The framework also adsorbed significantly more SO_2 in the presence of water than under dry conditions (4.5 ± 0.3 mmol/g; see Figure S5 and Table S1). This capacity corresponds to an uptake of approximately one SO_2 molecule per diamine, based on a diamine loading of 98% (as determined from solution ^1H NMR analysis of the digested framework). This approximate 1:1 stoichiometry was also confirmed by elemental analysis, which revealed a S/N mass ratio of 1.08, corresponding to 0.95 ± 0.1 SO_2 molecules per diamine (Table S3). While dmpn–Mg_2(dobpdc) still exhibited a step-shaped CO_2 uptake at 40 °C following saturation with humid SO_2, it retained only 75% of its original CO_2 capacity, considerably less than that retained after dry SO_2 exposure (Figure 2a). It is clear that humidity promotes at least partial deactivation of dmpn–Mg_2(dobpdc) in the presence of SO_2, consistent with previous studies of other amine-functionalized solids.[8,30]

Interestingly, when pristine dmpn–Mg_2(dobpdc) was exposed to a simulated flue gas stream containing 30 ppm
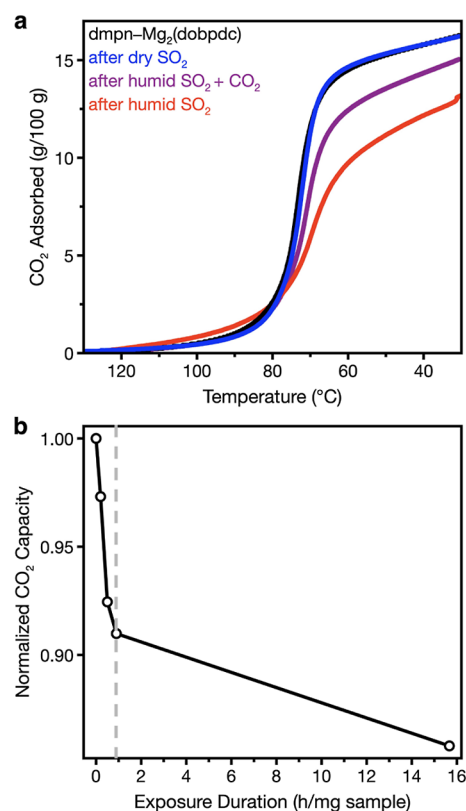

Figure 2. (a) Pure CO_2 adsorption isobars obtained at atmospheric pressure for pristine dmpn–Mg_2(dobpdc) before (light blue) and after saturation with the following gas streams at 40 °C and atmospheric pressure: dry 30 ppm SO_2 in N_2 (dark blue), 30 ppm SO_2 with 2% water in N_2 (red curve), and 30 ppm, 2% water, and 14% CO_2 in N_2 (purple curve). (b) Total CO_2 capacity retained by dmpn–Mg_2(dobpdc) based on isobar data obtained following exposure to a simulated coal flue gas (30 ppm SO_2, 14% CO_2, ~2% H_2O in N_2 at 40 °C and atmospheric pressure) under breakthrough conditions for various time durations. The gray dashed line represents the point at which SO_2 saturation occurs under these conditions.

SO_2, ~2% water, and 14% CO_2 in a balance of N_2 at atmospheric pressure and 40 °C, SO_2 breakthrough occurred in only 15 h, less than half the time required in the absence of CO_2. The SO_2 uptake under these conditions was also significantly less, only 1.4 ± 0.3 mmol/g or 0.4 ± 0.1 SO_2/diamine (Figure S5 and Table S1), revealing that the presence of CO_2 inhibits SO_2 binding significantly. Based on pure CO_2 isobar data collected following this breakthrough experiment, the framework retained 91% of its original CO_2 capacity at 40 °C (Figure 2a, purple curve). In addition, dmpn–Mg_2(dobpdc) retained 86% of its initial CO_2 capacity after exposure to the simulated flue gas stream for a duration corresponding to approximately 16 sequential breakthrough experiments (Figure 2b). This robust performance further highlights the potential of dmpn–Mg_2(dobpdc) as a candidate for CO_2 capture from coal flue gas streams.

To investigate dmpn–Mg_2(dobpdc) deactivation in the presence of humid SO_2, we used solution ^1H NMR spectroscopy and CHNS elemental analysis to analyze samples following humid SO_2 exposure and subsequent regeneration. Sample regeneration at 130 °C under dry, flowing N_2 was found to be optimal after testing a variety of conditions, including different temperatures and purge gas streams (Figures S8−S10). Analysis of ^1H NMR spectra collected for

237 digested framework samples following humid SO_2 exposure
238 before and after regeneration revealed that diamine loss
239 (~10%) occurs only upon regeneration. Elemental analysis of
240 dmpn−Mg_2(dobpdc) following humid SO_2 exposure and
241 regeneration revealed an N/C ratio consistent with this
242 diamine loss (Table S4) and an S/N ratio of 0.10,
243 corresponding to slightly less than 0.1 molecules of SO_2 per
244 diamine. Altogether, these results indicate that the diminished
245 CO_2 capacity of dmpn−Mg_2(dobpdc) following SO_2 exposure
246 is due to diamine loss upon regeneration and the persistence of
247 a small quantity of bound sulfur species.

248 Importantly, exposure of dmpn−Mg_2(dobpdc) to humid
249 SO_2 does not cause irreversible degradation of the underlying
250 framework. Indeed, powder X-ray diffraction analysis of a
251 sample of dmpn−Mg_2(dobpdc) following humid SO_2 exposure
252 and subsequent diamine stripping with methanol revealed a
253 powder pattern consistent with that obtained for pristine
254 Mg_2(dobpdc) (Figure S15). Further, N_2 adsorption data
255 obtained at 77 K for both samples revealed almost identical
256 surface areas of ~4200 m^2/g (Figure S16). This indicates that
257 the grafted amines protect the Mg_2(dobpdc) framework from
258 H_2O- and SO_2-induced poisoning at the metal sites.[50]
259 Importantly, this opens the possibility that the material could
260 potentially be occasionally regenerated in situ through
261 replacement of the diamines to regain capacity losses due to
262 extensive SO_2 exposure.

263 We next investigated the stability of dmpn−Mg_2(dobpdc) to
264 repeated cycling under the simulated flue gas stream (30 ppm
265 SO_2, 14% CO_2, ~2% H_2O, balance N_2 at atmospheric pressure
266 and 40 °C). Four cycles were carried out in total, and each
267 cycle consisted of exposure of the framework to the gas stream
268 until full breakthrough of SO_2 was observed, followed by
269 regeneration for 30 min under flowing N_2 at 130 °C and
270 atmospheric pressure (see Figure S6 and Table S2). After each
271 cycle, pure CO_2 adsorption isobars were collected (Figure 3a).
272 Over the course of the four cycles, the CO_2 capacity at 40 °C
273 was reduced by 21%, with the greatest capacity loss (10%)
274 occurring after the first cycle (Figure 3). The progressively
275 smaller losses in CO_2 capacity with each cycle number suggest
276 that this material may reach a stable CO_2 operating capacity in
277 the presence of SO_2 after initial passivation. This observation is
278 also supported by the diminished SO_2 uptake with increasing
279 cycle number (Figure 3b). Similar results were obtained from
280 SO_2 cycling experiments using a gas stream consisting of 30
281 ppm SO_2 and ~2% H_2O in N_2 at atmospheric pressure and 40
282 °C, indicating that, independent of CO_2, the framework affinity
283 for SO_2 uptake decreases with repeated cycling (see Figures
284 S12 and S13; Table S7). Analogous behavior has also been
285 reported for amine-silica materials cycled repeatedly with ppm
286 levels of dry SO_2, with and without CO_2.[28,29,51] In all, these
287 results further highlight the potential of dmpn−Mg_2(dobpdc)
288 for coal flue gas CO_2 capture applications. However, more
289 extended cycling tests are needed to substantiate this
290 performance along with evaluation of the CO_2 capture
291 performance in the presence of SO_2 during simulated flue
292 gas exposure.

293 **Spectroscopic Characterization of Humid SO_2 Ad-**
294 **sorption.** Infrared spectroscopy was used as an initial probe of
295 the species formed upon humid SO_2 uptake in dmpn−
296 Mg_2(dobpdc). Following saturation of the material with humid
297 SO_2, new peaks appeared at 913 and 864 cm^{-1} (Figure S14),
298 closely corresponding to the S−O stretching frequency of the
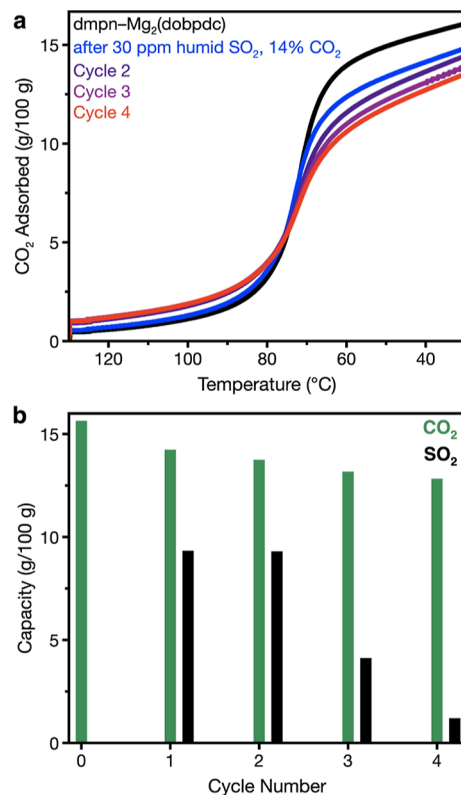299 sulfite ion and/or bisulfite ion (984 to 917 cm^{-1})[31,32,48,52−57]

Figure 3. (a) Pure CO_2 isobars collected at atmospheric pressure for dmpn−Mg_2(dobpdc) before (black curve) and after (colored curves) successive cycles of saturation with SO_2 using a gas stream containing 30 ppm SO_2, 2% water, and 14% CO_2 in N_2 at 40 °C and atmospheric pressure. Prior to isobar collection, the sample was regenerated under a flow of dry N_2 at 130 °C for 30 min. The material was then heated in the breakthrough apparatus to 100 °C under flowing N_2 at atmospheric pressure before the next cycle. (b) Comparison of the SO_2 capacities measured from SO_2 breakthrough experiments using a simulated coal flue gas and the CO_2 capacity at 40 °C determined from isobaric measurements following each SO_2 saturation cycle.

and the S−OH vibration of bisulfate or bisulfite (870 to 850 300
cm^{-1}), respectively.[31,32,55−57] Together, the appearance of 301
these new peaks suggests that SO_2 adsorbs in dmpn− 302
Mg_2(dobpdc) to form bisulfite ($HSO_3^−$). Liquid chromatog- 303
raphy−mass spectrometry analysis of the liquid solution 304
generated upon stripping the amines from dmpn− 305
Mg_2(dobpdc) following exposure to a humid 30 ppm SO_2 306
stream revealed the presence of the sulfite ion, which was not 307
present in a control sample prepared by stripping the amines 308
from pristine dmpn−Mg_2(dobpdc) (Figure S17). Because the 309
charge-inducing nature of ESI mass spectrometry does not 310
enable one to distinguish between sulfite and bisulfite ions, we 311
turned to solid-state magic angle spinning (MAS) NMR 312
spectroscopy and DFT calculations to make a more conclusive 313
assignment of the species formed upon SO_2 uptake in dmpn− 314
Mg_2(dobpdc). 315

The room-temperature solid-state ^{15}N NMR spectra for a 316
sample of dmpn−Mg_2(dobpdc) before and after saturation 317
with humid 30 ppm SO_2 are shown in Figure 4. The pristine 318
framework exhibits a single ^{15}N resonance at 12 ppm, as 319
determined previously.[24] While at any given time, there will be 320
two chemically distinct nitrogen atoms in the framework, 321
corresponding to the metal-bound and free amines, symmetric 322
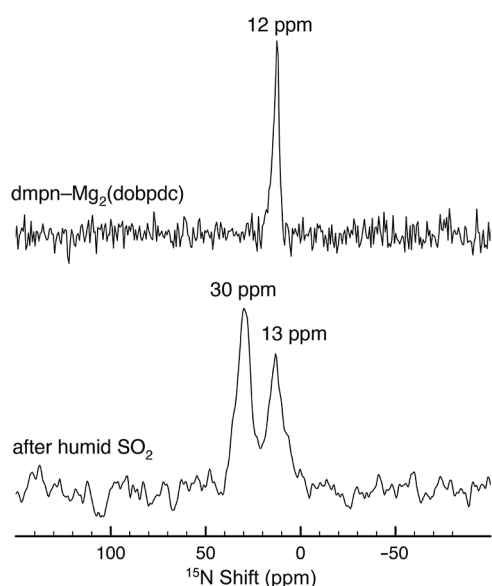diamines are known to exhibit only one ^{15}N resonance at room 323

Figure 4. Room-temperature ^{15}N solid-state MAS NMR spectra of pristine dmpn−Mg$_2$(dobpdc) (upper, 16.4 T, 15 kHz MAS rate) and dmpn−Mg$_2$(dobpdc) after saturation with a gas stream containing 30 ppm SO$_2$ and 2% water in N$_2$ (lower, 11.7 T, 10 kHz MAS rate). The spectrum for pristine dmpn−Mg$_2$(dobpdc) is reprinted with permission from ref 24. Copyright 2018, Journal of the American Chemical Society.

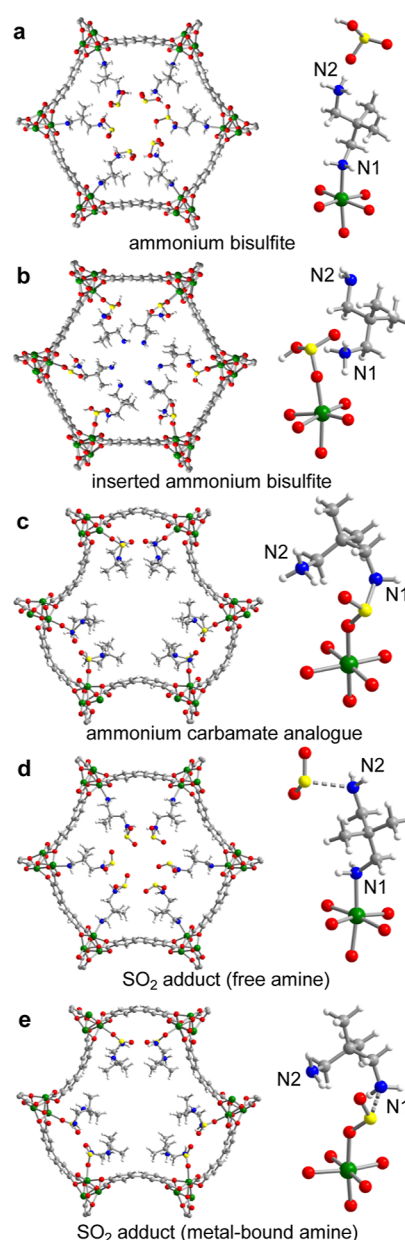temperature due to rapid exchange of the two sites.[24,58] Following saturation of the material with humid SO$_2$, the original amine resonance persists and a new ^{15}N resonance appears at 30 ppm, which was assigned to an ammonium species based on previous solid-state ^{15}N NMR characterization of ammonium formed in the material following CO$_2$ dosing.[24] Although these experiments were not quantitative, the retention of the original peak indicates that unreacted amines remain in the material following dosing with SO$_2$. Considering the previously quantified loading of one SO$_2$ for every diamine and the need to maintain charge balance, this result supports the formation of ammonium bisulfite ($-NH_3^+$ HSO_3^-) species.

We next turned to vdW-corrected DFT to further elucidate the chemical species formed upon uptake of humid SO$_2$ in dmpn−Mg$_2$(dobpdc) (see Section S12 of the Supporting Information for details). Based on the spectroscopic data, we initially considered an optimized ammonium bisulfite structure featuring bisulfite charge balanced by ammonium generated from the free end of the diamine (Figure 5a). This amine is expected to be more basic and less sterically encumbered than the metal-bound amine and therefore more likely to interact with SO$_2$. The predicted ^{15}N shifts for this species are 27 and 12 ppm, which correspond closely with the experimentally observed shifts of 30 and 13 ppm. The predicted chemical shifts for this structure were also the closest match to the experiment when compared with the shifts for several other hypothetical structures, including neutral SO$_2$ adducts and an analogue of the ammonium carbamate structure, with CO$_2$ replaced by SO$_2$, featuring direct bonds from an amine nitrogen to sulfur (Figure 5 and Table 1). We also considered a second ammonium bisulfite structure featuring a metal-bound bisulfite charge balanced by ammonium generated from the metal-bound amine (Figure 5b), although the calculated

Figure 5. Structures of candidate products formed upon humid SO$_2$ uptake in dmpn−Mg$_2$(dobpdc) generated from vdW-corrected DFT calculations: ammonium bisulfite formed upon reaction of SO$_2$ at the (a) free amine and (b) metal-bound amine, (c) SO$_2$ analogue of the ammonium carbamate structure formed in dmpn−Mg$_2$(dobpdc)[24] and an adduct of SO$_2$, and (d) free amine and (e) metal-bound amine. Green, gray, red, blue, yellow, and white spheres represent Mg, C, O, N, S, and H atoms, respectively.

^{15}N shifts for this species (32 and 5 ppm) show poorer agreement with the experimental data.

Owing to the broad nature of the experimental ^{15}N NMR resonances, it is not possible to exclude with confidence the latter structure based on these data alone. However, binding energies computed for the various SO$_2$-derived products using vdW−DFT further support ammonium bisulfite formation at the free amine. Indeed, this structure is the most stable of all examined products, and it is more stable by ∼50 kJ/mol compared to the metal-bound bisulfite structure (Table 1). It should be noted that our DFT approach for calculating binding energies neglects quantum zero-point and finite-temperature

E

Table 1. Predicted ^{15}N NMR Chemical Shifts and Binding Energies of Candidate Structures (See Figure 5) Formed Upon SO$_2$ Uptake in dmpn−Mg$_2$(dobpdc)

SO$_2$-derived product	calculated ^{15}N shift (ppm)		calculated binding energy (kJ/mol)
	N1	N2	
ammonium bisulfite	12	27	−148
inserted ammonium bisulfite	32	5	−98
ammonium carbamate analogue	128	28	−63
SO$_2$ adduct (free amine)	14	69	−70
SO$_2$ adduct (metal-bound amine)	81	19	−53

corrections associated with the nuclei. Based on prior studies of CO$_2$ uptake in various diamine−Mg$_2$(dobpdc) materials, the predicted binding energies deviate from isosteric heats of adsorption measured in the experiment; however, they do accurately capture measured trends.[15,20,59]

Effect of Diamine Structure on MOF Stability to SO$_2$. To further investigate the stability of alkyldiamine-appended Mg$_2$(dobpdc) materials to SO$_2$, we evaluated the CO$_2$ capture performance of several analogues featuring 1°,1°-, 1°,2°-, or 1°,3°-alkyldiamines (including dmen, i-2, and e-2 studied previously[22,23]) following saturation with a humid stream (2% H$_2$O) containing 30 ppm of SO$_2$ in N$_2$ (see Table 2 and Figure

S18). Notably, materials functionalized with 1°,1°-diamines— dmpn−Mg$_2$(dobpdc) and dmen−Mg$_2$(dobpdc)—were found to be the most stable to humid SO$_2$ based on the CO$_2$ capacity and diamine loading that were retained following SO$_2$ exposure and subsequent regeneration. Both of these materials are stable to water in contrast to the previously studied en− Mg$_2$(dobpdc),[22,23,27] which also features a 1°,1° amine. These preliminary results indicate that, contrary to what was proposed previously,[23] the presence of bulky substituents is not alone sufficient to rationalize the stability of diamine-appended Mg$_2$(dobpdc) to SO$_2$. However, of the 1°,2°- and 1°,3°-alkylamine-appended variants investigated here, those with larger secondary or tertiary amine substituents, namely, i-2−Mg$_2$(dobpdc) and ee-2−Mg$_2$(dobpdc) (ee-2 = N,N-diethylethylenediamine), were found to be more stable than their counterparts with smaller N-alkyl substituents. Thus, for diamines in the same class, the size of the alkyl substituents may also be an important factor, as discussed further below.

It was previously established that 1°,2°- and 1°,3°-diamines bind to the open metal sites of Mg$_2$(dobpdc) through the primary amine,[18] leaving the secondary or tertiary amine dangling into the framework pore. Separately, multiple studies of other amine-appended adsorbents have found that humid SO$_2$ often reacts irreversibly with primary amines and to a lesser degree with secondary amines, while it tends to bind reversibly to materials featuring tertiary amines.[30,39,60,61] We hypothesized that in 1°,2°- and 1°,3°-diamine-appended Mg$_2$(dobpdc), humid SO$_2$ may preferentially react with the

Table 2. Results of Stability Analysis for Diamine−Mg$_2$(dobpdc) after Saturation with a Gas Stream Containing 30 ppm SO$_2$ and 2% Water in N$_2$ at 40 °C and Atmospheric Pressure

Diamine (Abbreviation)	Structure	Class	Diamine Loading (%)[a]			CO$_2$ Capacity Retained (%)[c]
			Pristine	After Saturation with SO$_2$	After SO$_2$ and Regeneration[c]	
2,2-dimethyl-1,3-propanediamine (dmpn)		1°,1°	98	98	89	77
1,2-diamino-2-methylpropane (dmen)		1°,1°	97	91	75	75
N-ethylethyelenediamine (e-2)		1°,2°	98	92	52	39
N-isopropyl-ethylenediamine (i-2)		1°,2°	101	89	70	64
N,N-dimethylethylenediamine (mm-2)		1°,3°	92	68	59	34
N,N-dimethylpropoanediamine (mm-3)		1°,3°	97	75	68	38
N,N-diethylethylenediamine (ee-2)		1°,3°	97	66	65	53

[a]Determined from solution ^1H NMR data collected for digested samples. An error of ±2% was consistently determined for all samples based on standard deviation of three distinct diamine proton signals determined from two identically prepared samples. [b]Regeneration at 130 °C under flowing N$_2$ for 30 min. [c]Based on pure CO$_2$ isobars obtained after framework saturation with SO$_2$ and regeneration at 130 °C under flowing N$_2$ for 30 min. The error on each value is ±2% based on standard deviation of CO$_2$ capacity from three identically prepared samples.

metal-bound primary amine over the exposed but sterically hindered amines. This disruption of the metal–amine bond would in turn promote more facile degradation of the material relative to 1°,1°-diamine-appended variants, where SO_2 is expected to react preferentially with the free amine. To evaluate this possibility further, we collected solid-state MAS ^{15}N NMR spectra for e-2–Mg_2(dobpdc) and ee-2–Mg_2(dobpdc) as representative 1°,2°- and 1°,3°-diamine-appended frameworks before and after saturation with humid 30 ppm SO_2 in N_2 (Figure 6). The spectra of the pristine frameworks both feature two resonances, which were assigned to the chemically distinct primary and secondary/tertiary amines in the materials.[24] Saturation with humid SO_2 resulted in disappearance of the primary amine resonance for e-2–Mg_2(dobpdc) (Figure 6a), whereas in the case of ee-2–
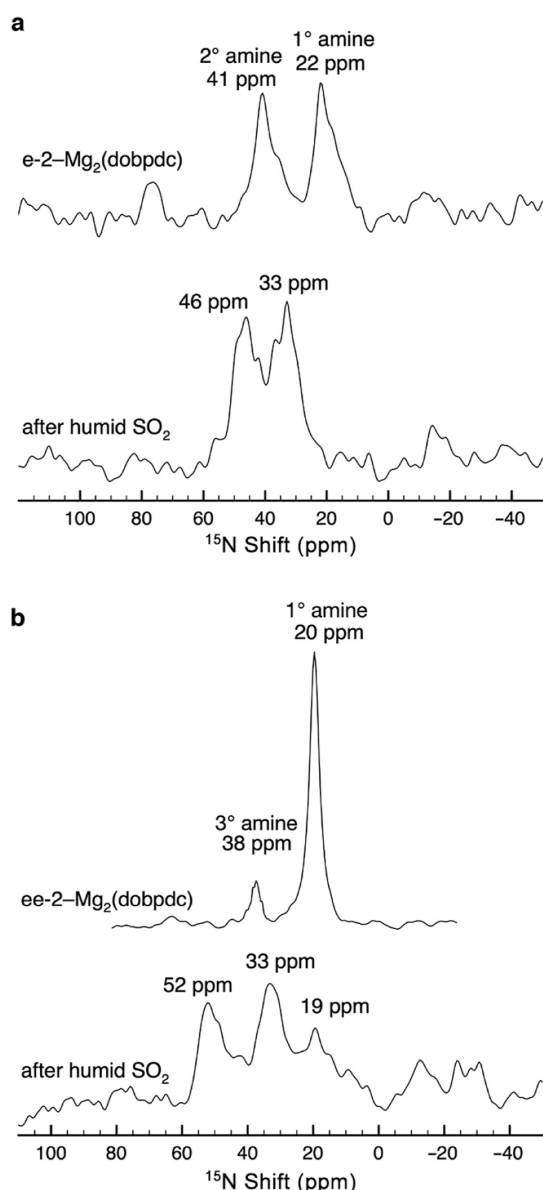

Figure 6. Room-temperature ^{15}N MAS NMR spectra of e-2–Mg_2(dobpdc) (a) and ee-2–Mg_2(dobpdc) (b) before and after saturation with a gas stream containing 30 ppm of SO_2 and 2% water in N_2. Experiments were conducted at 11.4 T with a MAS rate of 10 kHz.

Mg_2(dobpdc), this resonance was diminished but not absent (Figure 6b). For both materials, SO_2 exposure resulted in the appearance of a strong resonance at 33 ppm, which was assigned to a primary ammonium species, based on similar chemical shifts identified for primary ammonium species formed upon CO_2 uptake in diamine-appended Mg_2(dobpdc).[24] These results support protonation of the initially metal-bound primary amine in both materials following exposure to humid SO_2. The secondary amine peak for e-2–Mg_2(dobpdc) shifts from 41 to 46 ppm upon saturation of the material with humid SO_2, possibly a result of weak interactions between this amine and bisulfite. Similar interactions may lead to a more dramatic shift of the tertiary amine peak for ee-2–Mg_2(dobpdc) from 38 to 52 ppm after humid SO_2 saturation, although further experiments would be needed to make definitive assignments. Finally, following saturation with humid SO_2, the infrared spectra of both materials feature two new bands that support the presence of bisulfite (Figure S19).

We again turned to vdW–DFT to help elucidate the species formed upon saturation of e-2–Mg_2(dobpdc) and ee-2–Mg_2(dobpdc) with humid SO_2. Both materials experience substantial diamine loss following humid SO_2 exposure and regeneration (Table 2). However, e-2–Mg_2(dobpdc) retains a much higher diamine loading following humid SO_2 exposure, and as such the structure of this material with adsorbed SO_2 is presumed to be more uniform than that of ee-2–Mg_2(dobpdc). Accordingly, we used e-2–Mg_2(dobpdc) as the model framework for our calculations. Based on the ^{15}N NMR and IR data for e-2–Mg_2(dobpdc) and the evidence of ammonium bisulfite formation (Figures 6 and S19), we evaluated two possible structures formed upon SO_2 uptake, featuring ammonium bisulfite formed at the site of the dangling amine or bisulfite inserted into the metal–amine bond and stabilized by a primary ammonium cation (see Figure S23 and Table S8). Interestingly, the predicted chemical shifts for the structure resulting from protonation of the primary metal-bound amine and its displacement by bisulfite (34 and 52 ppm) are in better agreement with the experimental shifts than those for the structure with bisulfite and a dangling secondary ammonium (17 and 48 ppm). This result contrasts with the reactivity determined for dmpn–Mg_2(dobpdc), where bisulfite forms an ion pair with ammonium generated from the free amine. In all, these results support the hypothesis that 1°,2°- (and by extension 1°,3°-) diamine-appended Mg_2(dobpdc) materials are less robust to humid SO_2 than 1°,1°-diamine-appended variants, owing to the preferential reaction of humid SO_2 with the metal-bound primary amine and disruption of the critical metal–nitrogen linkage in these materials. As noted above, the trends in Table 2 additionally indicate that bulkier diamines within the same class are more stable to humid SO_2. Among diamines that bind through a primary amine, heavier analogues are known to be more thermally stable and volatilize at higher temperatures.[18] This stability may translate to decreased diamine loss during SO_2 exposure and subsequent regeneration.

■ CONCLUSIONS

We have carried out an in-depth investigation of the effect of humid SO_2 exposure on the stability and CO_2 adsorption properties of the MOF dmpn–Mg_2(dobpdc), a promising candidate for CO_2 capture from coal flue gas.[19] Using a custom-built SO_2 breakthrough apparatus, we found that this

G

material exhibits excellent stability to dry and humid SO_2. In particular, the material exhibits no loss in CO_2 capacity following saturation with a stream containing 30 ppm SO_2 in N_2 and only a 25% loss in CO_2 capacity following saturation with a stream of humid 30 ppm SO_2 in N_2. Importantly, this capacity loss is reduced to under 10% when dmpn−Mg_2(dobpdc) is exposed to humid 30 ppm SO_2 in the presence of 14% CO_2. Further, preliminary cycling experiments performed using a simulated flue gas (30 ppm SO_2, 14% CO_2, ~2% H_2O in N_2) indicate that the CO_2 capacity may stabilize around 80% after initial SO_2-induced passivation. In all, these results are promising compared to the few studies that have been conducted on other amine-appended adsorbents under relevant SO_2 concentrations, and they further highlight the potential of dmpn−Mg_2(dobpdc) for CO_2 capture applications.

Characterization of dmpn−Mg_2(dobpdc) following humid SO_2 exposure using IR and ^{15}N NMR spectroscopy, supported by vdW−DFT calculations, revealed that SO_2 reacts with the free end of the metal-bound diamine to form ammonium bisulfite species. To the best of our knowledge, these results afford the most comprehensive evidence to date of the formation of ammonium bisulfite in amine-functionalized materials upon reaction with humid SO_2. Spectroscopic and DFT analyses of several other diamine-appended Mg_2(dobpdc) variants revealed that SO_2 preferentially reacts with the metal-bound primary amine in variants featuring 1°,2°- or 1°,3°-diamines—due to weaker interactions between SO_2 and the pore-dwelling N-alkylated amines—forming a metal-bound bisulfite charge balanced by a primary ammonium cation. This disruption of the metal−amine bond is likely what renders these materials significantly less stable to SO_2 than the 1°,1°-diamine-appended variants studied here, including dmpn−Mg_2(dobpdc). Knowledge of this critical structure−property relationship will support the design of more robust amine-appended frameworks for carbon capture from coal flue gas and, more generally, for the capture of CO_2 from other industrially relevant exhaust streams (e.g., from cement manufacturing and biofuel combustion), which contain similar SO_2 concentrations to those investigated here.[62,63]

■ EXPERIMENTAL SECTION

General Procedures. All solvents and reagents were purchased from commercial sources and used without further purification. The linker H_4dobpdc was purchased from Hangzhou Trylead Chemical Technology Co. Ultrahigh purity (>99.998%) gases were used for all adsorption measurements, with custom mixtures purchased from Praxair. Powder X-ray diffraction (PXRD) patterns were collected on a Bruker ADVANCE D8 diffractometer equipped with a Cu Kα source operating at 40 kV, 40 mA. Elemental analysis was conducted at the Microanalytical Facility at UC Berkeley. Attenuated total reflectance Fourier transform infrared spectra were collected in air on a PerkinElmer Spectrum 400 Fourier transform IR equipped with a Pike GladiATR module.

Synthesis of Mg_2(dobpdc). The framework Mg_2(dobpdc) was produced following a previously reported solvothermal synthesis.[18] Briefly, $Mg(NO_3)_2$ (5.75 g, 22.5 mmol, 1.24 equiv) and H_4dobpdc (4.95 g, 18.0 mmol, 1.00 equiv) were added to 100 mL of a 55:45 methanol/N,N-dimethylformamide (v/v) solution. This mixture was sonicated until all solids completely dissolved and then gravity filtered to ensure removal of any particulates. The solution was then transferred to a glass pressure vessel with a stir bar and heated to 120 °C in an oil bath for 20 h under constant stirring. The resulting white powder was then isolated by vacuum filtration and washed three times at 60 °C for at least 3 h each in 300 mL of fresh N,N-

dimethylformamide per wash. A solvent exchange was then performed with three subsequent washes at 60 °C for at least 3 h each in 300 mL of fresh methanol per wash. The washed material was then isolated again through vacuum filtration and stored in fresh methanol. The framework was desolvated prior to characterization by heating under flowing N_2 at 180 °C for a minimum of 3 h, followed by heating at 180 °C under vacuum overnight. Langmuir surface area and PXRD data were consistent with previously published values[17,18] and are presented in Figures S1 and S2.

Synthesis of Diamine-Appended Mg_2(dobpdc). Diamines were appended onto the open metal sites of the Mg_2(dobpdc) framework following an adaptation of a previously reported procedure.[19] Approximately, 30 mg of Mg_2(dobpdc) was isolated from methanol using vacuum filtration and left to dry on the filter over vacuum until the powder was no longer moist, typically no more than 5 min. This powder was then washed with 20 mL of fresh toluene before being transferred to a scintillation vial charged with a solution of 1 mL of diamine in 4 mL of toluene. After 16 h at room temperature, the powder was isolated by vacuum filtration and washed with 20 mL of fresh toluene over the filter paper. The resulting diamine-appended material was then activated at 130 °C under flowing N_2 for 30 min to remove the solvent and excess diamine before use. Diamine loading was then assessed using ^{1}H NMR spectroscopy and collected on a Bruker AVQ-400 instrument (see Table 2). In these measurements, roughly 5 mg of diamine-appended Mg_2(dobpdc) material was suspended in 1 mL of DMSO-d_6 and dissolved by the subsequent addition of 20 μL of 35 wt % DCl in D_2O solution. These solutions were sealed in a 4 mL vial and heated at 60 °C until complete dissolution of solids was achieved.

Thermogravimetric Analysis. Thermogravimetric CO_2 isobars were measured at atmospheric pressure using a TA Instruments TGA Q5000. An aliquot (~5 mg) of the material was activated in the instrument at 130 °C under flowing N_2 for 30 min before isobaric measurements were conducted under 100% CO_2 at a temperature ramp rate of 1 °C/min. Thermal decompositions were conducted under pure N_2 at a 1.5 °C/min ramp rate. All CO_2 capacity values are based on the gravimetric uptake in a pure, dry CO_2 isobar at 40 °C, the target coal flue gas capture temperature.

SO_2 Exposure. A custom-built corrosive gas exposure system (see Figure S3 and Section S3 of the Supporting Information) was used for saturation of samples with humid SO_2 under dilute and precisely controllable conditions. A sample of activated diamine−Mg_2(dobpdc) was loaded into the bed in air as a loose powder and heated in the exposure system under 50 sccm of dry N_2 at 100 °C for 1 h to remove any gases adsorbed during air exposure. The bed was then cooled to 40 °C under N_2, and the gas stream was then switched to 50 sccm of 30 ppm humid (~2% H_2O) or dry SO_2 in N_2, as specified for each experiment. All exposure experiments were conducted using a flow rate of 50 sccm at 40 °C and a total pressure of 1 atm. The custom gas mixture was flowed continuously over the adsorbent bed until the Tango TX-1 SO_2 detector measured the outlet concentration of SO_2 as equivalent to the inlet concentration, indicating full material saturation with SO_2. The adsorbent bed was then purged with 50 sccm of dry N_2 to remove any excess free SO_2 while cooling to room temperature before the bed was opened, and the sample was recovered for subsequent testing.

The incorporation of CO_2 is possible via a three-way valve connecting a gas cylinder containing 15% CO_2 in N_2 to the inert gas mass flow controller. Upon blending this mixture with the SO_2-containing stream, the final test conditions were 30 ppm SO_2, 14% CO_2, ~2% H_2O, balance N_2 at the same temperature and flow rate. The bubbler water was exchanged following any change in the gas stream composition to eliminate contamination from dissolved gases. The SO_2 detector was used to ensure that the bubbler was completely saturated with SO_2 before starting any exposure tests. The inlet gas stream is humidified by a single 20-ounce bubbler with a fritted dispersion tube for all humid tests. This stream is assumed to be saturated with water at room temperature (20 °C), yielding a ~2.3% H_2O content and 32% RH at 40 °C. Stainless steel (316 grade) and

corrosion-resistant coatings were used in all parts of this apparatus to ensure stability to dry and humid SO_2.

All SO_2 exposure experiments were conducted under 30 ppm of SO_2 unless otherwise stated. Dry SO_2 exposure experiments at concentrations above 30 ppm were conducted using the same system without the outlet SO_2 detector due to its incompatibility with the elevated concentrations. Instead, the flow time was calculated based on a 1 or 2 SO_2 per diamine ratio using the sample mass, stream concentration, and flow rate (Figure S7).

The SO_2 capacity was calculated from the measured breakthrough curves following analysis presented in Section S3 of the Supporting Information.

Diamine Stripping from Diamine–Mg₂(dobpdc). Diamine molecules were removed from the $Mg_2(dobpdc)$ framework by soaking in methanol at room temperature for 2 h, followed by isolation of the framework powder through vacuum filtration. Complete removal of diamines was confirmed by ^1H NMR spectroscopy.

Mass Spectrometry. The recovered methanol solution from diamine stripping was analyzed using an HR-LCMS, the Agilent 6545 AJS-ESI QToF. A 100% acetonitrile mobile solvent was used with a reverse-phase C18 column at a flow rate of 0.5 mL/min. A 1 μL sample was injected at 1.25 g/L. The solution recovered from a humid SO_2-exposed dmpn–$Mg_2(dobpdc)$ sample was analyzed. A control solution was also produced by stripping the diamines from an untreated dmpn–$Mg_2(dobpdc)$ sample. The mass spectra of the control and treated solutions were compared using Mass Hunter qualitative analysis.

DFT Methods. DFT methods are reported in Section S12 of the Supporting Information.

Solid-State NMR Methods. Solid-state NMR methods are reported in Section S13 of the Supporting Information. All samples were studied using the natural ^{15}N isotopic abundance and were not further enriched.

■ ASSOCIATED CONTENT

Ⓢ Supporting Information

The Supporting Information is available free of charge at https://pubs.acs.org/doi/10.1021/jacs.2c07498.

Characterization of Mg2(dobpdc); estimation of SO2 concentration in coal flue gas; SO2 breakthrough apparatus and results; exposure of dmpn–Mg2(dobpdc) to various concentrations of dry SO2; CHNS elemental analysis; evaluation of optimal regeneration conditions for dmpn–Mg2(dobpdc) following humid SO2 exposure; humid SO2 cycling and extended exposure with dmpn–Mg2(dobpdc); spectroscopic characterization of dmpn–Mg2(dobpdc) before and after humid SO2 saturation; characterization of Mg2(dobpdc) following SO2 saturation and diamine stripping; mass spectrometry; CO2 isobar profiles for diamine–Mg2(dobpdc) obtained after saturation with humid SO2; density functional theory calculations; and solid-state NMR methods (PDF)

Computationally generated hypothetical SO2 product structures used for predicted ^{15}N NMR calculations (ZIP)

■ AUTHOR INFORMATION

Corresponding Author

Jeffrey R. Long − Department of Chemical and Biomolecular Engineering, University of California Berkeley, Berkeley, California 94720, United States; Materials Sciences Division, Lawrence Berkeley National Laboratory, Berkeley, California 94720, United States; Department of Chemistry, University of California Berkeley, Berkeley, California 94720, United States; ⓞ orcid.org/0000-0002-5324-1321; Email: jrlong@berkeley.edu

Authors

Surya T. Parker − Department of Chemical and Biomolecular Engineering, University of California Berkeley, Berkeley, California 94720, United States; Materials Sciences Division, Lawrence Berkeley National Laboratory, Berkeley, California 94720, United States; ⓞ orcid.org/0000-0001-8534-8361

Alex Smith − Department of Physics, University of California Berkeley, Berkeley, California 94720, United States

Alexander C. Forse − Department of Chemical and Biomolecular Engineering, University of California Berkeley, Berkeley, California 94720, United States; Present Address: Department of Chemistry, University of Cambridge, Cambridge, CB2 1EW, U.K; ⓞ orcid.org/0000-0001-9592-9821

Wei-Chih Liao − Department of Chemical and Biomolecular Engineering, University of California Berkeley, Berkeley, California 94720, United States

Florian Brown-Altvater − Department of Chemistry, University of California Berkeley, Berkeley, California 94720, United States; Molecular Foundry, Lawrence Berkeley National Laboratory, Berkeley, California 94720, United States

Rebecca L. Siegelman − Materials Sciences Division, Lawrence Berkeley National Laboratory, Berkeley, California 94720, United States; Department of Chemistry, University of California Berkeley, Berkeley, California 94720, United States; Present Address: DuPont de Nemours, Inc. 200 Powder Mill Rd, Wilmington, DE, 19803, United States.; ⓞ orcid.org/0000-0002-4249-6118

Eugene J. Kim − Department of Chemistry, University of California Berkeley, Berkeley, California 94720, United States; Present Address: Intel Corporation, Hillsboro, OR, 97124, United States.

Nicholas A. Zill − Department of Chemical and Biomolecular Engineering, University of California Berkeley, Berkeley, California 94720, United States

Wenjun Zhang − Department of Chemical and Biomolecular Engineering, University of California Berkeley, Berkeley, California 94720, United States; ⓞ orcid.org/0000-0001-9348-972X

Jeffrey B. Neaton − Materials Sciences Division, Lawrence Berkeley National Laboratory, Berkeley, California 94720, United States; Department of Physics, University of California Berkeley, Berkeley, California 94720, United States; Kavli Energy NanoSciences Institute at Berkeley, Berkeley, California 94720, United States

Jeffrey A. Reimer − Department of Chemical and Biomolecular Engineering, University of California Berkeley, Berkeley, California 94720, United States; Materials Sciences Division, Lawrence Berkeley National Laboratory, Berkeley, California 94720, United States; ⓞ orcid.org/0000-0002-4191-3725

Complete contact information is available at:
https://pubs.acs.org/10.1021/jacs.2c07498

Notes

The authors declare the following competing financial interest(s): The authors declare the following competing financial inter-est: J.R.L. has a financial interest in Mosaic

Materials, Inc., a start-up company working to commercialize metalorganic frameworks for gas separations.

■ REFERENCES

(1) Friedlingstein, P.; Jones, M. W.; O'Sullivan, M.; Andrew, R. M.; Hauck, J.; Peters, G. P.; Peters, W.; Pongratz, J.; Sitch, S.; Le Quéré, C.; Bakker, D. C. E.; Canadell, J. G.; Ciais, P.; Jackson, R. B.; Anthoni, P.; Barbero, L.; Bastos, A.; Bastrikov, V.; Becker, M.; Bopp, L.; Buitenhuis, E.; Chandra, N.; Chevallier, F.; Chini, L. P.; Currie, K. I.; Feely, R. A.; Gehlen, M.; Gilfillan, D.; Gkritzalis, T.; Goll, D. S.; Gruber, N.; Gutekunst, S.; Harris, I.; Haverd, V.; Houghton, R. A.; Hurtt, G.; Ilyina, T.; Jain, A. K.; Joetzjer, E.; Kaplan, J. O.; Kato, E.; Klein Goldewijk, K.; Korsbakken, J. I.; Landschützer, P.; Lauvset, S. K.; Lefèvre, N.; Lenton, A.; Lienert, S.; Lombardozzi, D.; Marland, G.; McGuire, P. C.; Melton, J. R.; Metzl, N.; Munro, D. R.; Nabel, J. E. M. S.; Nakaoka, S.-I.; Neill, C.; Omar, A. M.; Ono, T.; Peregon, A.; Pierrot, D.; Poulter, B.; Rehder, G.; Resplandy, L.; Robertson, E.; Rödenbeck, C.; Séférian, R.; Schwinger, J.; Smith, N.; Tans, P. P.; Tian, H.; Tilbrook, B.; Tubiello, F. N.; van der Werf, G. R.; Wiltshire, A. J.; Zaehle, S. Global Carbon Budget 2019. *Earth Syst. Sci. Data* **2019**, *11*, 1783−1838.

(2) *Global Energy and CO$_2$ Status Report*; International Energy Agency, 2019.

(3) Bui, M.; Adjiman, C. S.; Bardow, A.; Anthony, E. J.; Boston, A.; Brown, S.; Fennell, P. S.; Fuss, S.; Galindo, A.; Hackett, L. A.; Hallett, J. P.; Herzog, H. J.; Jackson, G.; Kemper, J.; Krevor, S.; Maitland, G. C.; Matuszewski, M.; Metcalfe, I. S.; Petit, C.; Puxty, G.; Reimer, J.; Reiner, D. M.; Rubin, E. S.; Scott, S. A.; Shah, N.; Smit, B.; Trusler, J. P. M.; Webley, P.; Wilcox, J.; Mac Dowell, N. Carbon Capture and Storage (CCS): The Way Forward. *Energy Environ. Sci.* **2018**, *11*, 1062−1176.

(4) Wang, M.; Lawal, A.; Stephenson, P.; Sidders, J.; Ramshaw, C. Post-Combustion CO$_2$ Capture with Chemical Absorption: A State-of-the-art Review. *Chem. Eng. Res. Des.* **2011**, *89*, 1609−1624.

(5) Chen, C.; Zhang, S.; Row, K. H.; Ahn, W.-S. Amine−Silica Composites for CO$_2$ Capture: A Short Review. *J. Energy Chem.* **2017**, *26*, 868−880.

(6) Lee, S.-Y.; Park, S.-J. A Review on Solid Adsorbents for Carbon Dioxide Capture. *J. Ind. Eng. Chem.* **2015**, *23*, 1−11.

(7) Choi, S.; Drese, J. H.; Jones, C. W. Adsorbent Materials for Carbon Dioxide Capture from Large Anthropogenic Point Sources. *ChemSusChem* **2009**, *2*, 796−854.

(8) Lashaki, M. J.; Khiavi, S.; Sayari, A. Stability of Amine-Functionalized CO$_2$ Adsorbents: a Multifaceted Puzzle. *Chem. Soc. Rev.* **2019**, *48*, 3320−3405.

(9) Furukawa, H.; Cordova, K. E.; O'Keeffe, M.; Yaghi, O. M. The Chemistry and Applications of Metal-Organic Frameworks. *Science* **2013**, *341*, 1230444.

(10) Bollini, P.; Didas, S. A.; Jones, C. W. Amine-Oxide Hybrid Materials for Acid Gas Separations. *J. Mater. Chem.* **2011**, *21*, 15100−15120.

(11) D'Alessandro, D. M.; Smit, B.; Long, J. R. Carbon Dioxide Capture: Prospects for New Materials. *Angew. Chem., Int. Ed.* **2010**, *49*, 6058−6082.

(12) Samanta, A.; Zhao, A.; Shimizu, G. K. H.; Sarkar, P.; Gupta, R. Post-Combustion CO$_2$ Capture Using Solid Sorbents: A Review. *Ind. Eng. Chem. Res.* **2012**, *51*, 1438−1463.

(13) Sumida, K.; Rogow, D. L.; Mason, J. A.; McDonald, T. M.; Bloch, E. D.; Herm, Z. R.; Bae, T.-H.; Long, J. R. Carbon Dioxide Capture in Metal-Organic Frameworks. *Chem. Rev.* **2012**, *112*, 724−781.

(14) Gomes, V. G.; Yee, K. W. K. Pressure Swing Adsorption for Carbon Dioxide Sequestration from Exhaust Gases. *Sep. Purif. Technol.* **2002**, *28*, 161−171.

(15) Kim, E. J.; Siegelman, R. L.; Jiang, H. Z. H.; Forse, A. C.; Lee, J.-H.; Martell, J. D.; Milner, P. J.; Falkowski, J. M.; Neaton, J. B.; Reimer, J. A.; Weston, S. C.; Long, J. R. Cooperative carbon capture and steam regeneration with tetraamine-appended metal-organic frameworks. *Science* **2020**, *369*, 392−396.

(16) McDonald, T. M.; Lee, W. R.; Mason, J. A.; Wiers, B. M.; Hong, C. S.; Long, J. R. Capture of Carbon Dioxide from Air and Flue Gas in the Alkylamine-Appended Metal−Organic Framework mmen−Mg$_2$(dobpdc). *J. Am. Chem. Soc.* **2012**, *134*, 7056−7065.

(17) McDonald, T. M.; Mason, J. A.; Kong, X.; Bloch, E. D.; Gygi, D.; Dani, A.; Crocellà, V.; Giordanino, F.; Odoh, S. O.; Drisdell, W. S.; Vlaisavljevich, B.; Dzubak, A. L.; Poloni, R.; Schnell, S. K.; Planas, N.; Lee, K.; Pascal, T.; Wan, L. F.; Prendergast, D.; Neaton, J. B.; Smit, B.; Kortright, J. B.; Gagliardi, L.; Bordiga, S.; Reimer, J. A.; Long, J. R. Cooperative Insertion of CO$_2$ in Diamine-Appended Metal−Organic Frameworks. *Nature* **2015**, *519*, 303−308.

(18) Siegelman, R. L.; McDonald, T. M.; Gonzalez, M. I.; Martell, J. D.; Milner, P. J.; Mason, J. A.; Berger, A. H.; Bhown, A. S.; Long, J. R. Controlling Cooperative CO$_2$ Adsorption in Diamine-Appended Mg$_2$(dobpdc) Metal−Organic Frameworks. *J. Am. Chem. Soc.* **2017**, *139*, 10526−10538.

(19) Milner, P. J.; Siegelman, R. L.; Forse, A. C.; Gonzalez, M. I.; Runčevski, T.; Martell, J. D.; Reimer, J. A.; Long, J. R. A Diaminopropane-Appended Metal−Organic Framework Enabling Efficient CO$_2$ Capture from Coal Flue Gas via a Mixed Adsorption Mechanism. *J. Am. Chem. Soc.* **2017**, *139*, 13541−13553.

(20) Siegelman, R. L.; Milner, P. J.; Forse, A. C.; Lee, J.-H.; Colwell, K. A.; Neaton, J. B.; Reimer, J. A.; Weston, S. C.; Long, J. R. Water Enables Efficient CO$_2$ Capture from Natural Gas Flue Emissions in an Oxidation-Resistant Diamine-Appended Metal−Organic Framework. *J. Am. Chem. Soc.* **2019**, *141*, 13171−13186.

(21) Martell, J. D.; Zasada, L. B.; Forse, A. C.; Siegelman, R. L.; Gonzalez, M. I.; Oktawiec, J.; Runčevski, T.; Xu, J.; Srebro-Hooper, M.; Milner, P. J.; Colwell, K. A.; Autschbach, J.; Reimer, J. A.; Long, J. R. Enantioselective Recognition of Ammonium Carbamates in a Chiral Metal-Organic Framework. *J. Am. Chem. Soc.* **2017**, *139*, 16000−16012.

(22) Jo, H.; Lee, W. R.; Kim, N. W.; Jung, H.; Lim, K. S.; Kim, J. E.; Kang, D. W.; Lee, H.; Hiremath, V.; Seo, J. G.; Jin, H.; Moon, D.; Han, S. S.; Hong, C. S. Fine-Tuning of the Carbon Dioxide Capture Capability of Diamine-Grafted Metal-Organic Framework Adsorbents Through Amine Functionalization. *ChemSusChem* **2017**, *10*, 541−550.

(23) Lee, W. R.; Kim, J. E.; Lee, S. J.; Kang, M.; Kang, D. W.; Lee, H. Y.; Hiremath, V.; Seo, J. G.; Jin, H.; Moon, D.; Cho, M.; Jung, Y.; Hong, C. S. Diamine-Functionalization of a Metal-Organic Framework Adsorbent for Superb Carbon Dioxide Adsorption and Desorption Properties. *ChemSusChem* **2018**, *11*, 1694−1707.

(24) Forse, A. C.; Milner, P. J.; Lee, J.; Redfearn, H. N.; Oktawiec, J.; Siegelman, R. L.; Martell, D.; Dinakar, B.; Zasada, L. B.; Gonzalez, M.

I.; Neaton, B.; Long, R.; Reimer, A. Elucidating CO$_2$ Chemisorption in Diamine-Appended Metal−Organic Frameworks. *J. Am. Chem. Soc.* **2018**, *140*, 18016−18031.

(25) Hughes, R.; Kotamreddy, G.; Ostace, A.; Bhattacharyya, D.; Siegelman, R. L.; Parker, S. T.; Didas, S. A.; Long, J. R.; Omell, B.; Matuszewski, M. Isotherm, Kinetic, Process Modeling, and Techno-Economic Analysis of a Diamine-Appended Metal−Organic Framework for CO$_2$ Capture Using Fixed Bed Contactors. *Energy Fuels* **2021**, *35*, 6040−6055.

(26) Lee, W. R.; Hwang, S. Y.; Ryu, D. W.; Lim, K. S.; Han, S. S.; Moon, D.; Choi, J.; Hong, C. S. Diamine-Functionalized Metal−Organic Framework: Exceptionally High CO$_2$ Capacities from Ambient Air and Flue Gas, Ultrafast CO$_2$ Uptake Rate, and Adsorption Mechanism. *Energy Environ. Sci.* **2014**, *7*, 744−751.

(27) Lee, W. R.; Jo, H.; Yang, L.-M.; Lee, H.; Ryu, D. W.; Lim, K. S.; Song, J. H.; Min, D. Y.; Han, S. S.; Seo, J. G.; Park, Y. K.; Moon, D.; Hong, C. S. Exceptional CO$_2$ Working Capacity in a Heterodiamine-Grafted Metal−Organic Framework. *Chem. Sci.* **2015**, *6*, 3697−3705.

(28) Rezaei, F.; Jones, C. W. Stability of Supported Amine Adsorbents to SO$_2$ and NO$_x$ in Postcombustion CO$_2$ Capture. 1. Single-Component Adsorption. *Ind. Eng. Chem. Res.* **2013**, *52*, 12192−12201.

(29) Rezaei, F.; Jones, C. W. Stability of Supported Amine Adsorbents to SO$_2$ and NO$_x$ in Postcombustion CO$_2$ Capture. 2. Multicomponent Adsorption. *Ind. Eng. Chem. Res.* **2014**, *53*, 12103−12110.

(30) Fan, Y.; Rezaei, F.; Labreche, Y.; Lively, R. P.; Koros, W. J.; Jones, C. W. Stability of Amine-Based Hollow Fiber CO$_2$ Adsorbents in the Presence of NO and SO$_2$. *Fuel* **2015**, *160*, 153−164.

(31) Bhattacharyya, S.; Pang, S. H.; Dutzer, M. R.; Lively, R. P.; Walton, K. S.; Sholl, D. S.; Nair, S. Interactions of SO$_2$-Containing Acid Gases with ZIF-8: Structural Changes and Mechanistic Investigations. *J. Phys. Chem. C* **2016**, *120*, 27221−27229.

(32) Bhattacharyya, S.; Han, R.; Kim, W.-G.; Chiang, Y.; Jayachandrababu, K. C.; Hungerford, J. T.; Dutzer, M. R.; Ma, C.; Walton, K. S.; Sholl, D. S.; Nair, S. Acid Gas Stability of Zeolitic Imidazolate Frameworks: Generalized Kinetic and Thermodynamic Characteristics. *Chem. Mater.* **2018**, *30*, 4089−4101.

(33) *Cost and Performance Baseline for Fossil Energy Plants. Vol. 1a: Bituminous Coal (PC) and Natural Gas to Electricity*. Revision 3; DOE/NETL-2015/1723; U.S. Department of Energy, National Energy Technology Laboratory, 2015.

(34) Yang, J.; Yu, X.; Yan, J.; Tu, S.-T.; Dahlquist, E. Effects of SO$_2$ on CO$_2$ Capture Using a Hollow Fiber Membrane Contactor. *Appl. Energy* **2013**, *112*, 755−764.

(35) National Energy Technology Laboratory. Post-Combustion CO$_2$ Capture. https://netl.doe.gov/coal/carbon-capture/post-combustion (accessed Nov 15, 2021).

(36) United States Environmental Protection Agency. Data Explorer. https://www.epa.gov/egrid/data-explorer (accessed Nov 15, 2021).

(37) Devilbis, J.; Ray, S. Sulfur Dioxide Emissions from U.S. Power Plants Have Fallen Faster than Coal Generation; U.S. Energy Information Administration, 2017. https://www.eia.gov/todayinenergy/detail.php?id=29812 (accessed Nov 15, 2021).

(38) *Cost and Performance Baseline for Fossil Energy Plants. Vol. 1: Bituminous Coal and Natural Gas to Electricity*; NETL-PUB-22638; U.S. Department of Energy, National Energy Technology Laboratory, 2019.

(39) Kim, C.; Choi, W.; Choi, M. SO$_2$-Resistant Amine-Containing CO$_2$ Adsorbent with a Surface Protection Layer. *ACS Appl. Mater. Interfaces* **2019**, *11*, 16586−16593.

(40) *Air Pollution Control Technology Fact Sheet*; EPA-452/F-03-034; U.S. Environmental Protection Agency.

(41) Hoydick, M. T.; Jansson, H. Increasing Wet FGD SO$_2$ Removal Efficiency; Power Engineering, 2015. https://www.power-eng.com/news/increasing-wet-fgd-so2-removal-efficiency/#gref. (accessed Nov 15, 2021).

(42) Ramezan, M.; Skone, T. J. *Carbon Dioxide Capture from Existing Coal-Fired Power Plants*; DOE/NETL-401/110907; National Energy Technology Laboratory, 2006.

(43) Lee, J.-Y.; Keener, T. C.; Yang, Y. J. Potential Flue Gas Impurities in Carbon Dioxide Streams Separated from Coal-Fired Power Plants. *J. Air Waste Manage. Assoc.* **2009**, *59*, 725−732.

(44) Hallenbeck, A. P.; Kitchin, J. R. Effects of O$_2$ and SO$_2$ on the Capture Capacity of a Primary-Amine Based Polymeric CO$_2$ Sorbent. *Ind. Eng. Chem. Res.* **2013**, *52*, 10788−10794.

(45) Granite, E. J.; Pennline, H. W. Photochemical Removal of Mercury from Flue Gas. *Ind. Eng. Chem. Res.* **2002**, *41*, 5470−5476.

(46) Belmabkhout, Y.; Sayari, A. Isothermal Versus Non-Isothermal Adsorption-Desorption Cycling of Triamine-Grafted Pore-Expanded MCM-41 Mesoporous Silica for CO$_2$ Capture from Flue Gas. *Energy Fuels* **2010**, *24*, 5273−5280.

(47) Liu, Y.; Ye, Q.; Shen, M.; Shi, J.; Chen, J.; Pan, H.; Shi, Y. Carbon Dioxide Capture by Functionalized Solid Amine Sorbents with Simulated Flue Gas Conditions. *Environ. Sci. Technol.* **2011**, *45*, 5710−5716.

(48) Liu, Q.; Xiong, B.; Shi, J.; Tao, M.; He, Y.; Shi, Y. Enhanced Tolerance to Flue Gas Contaminants on Carbon Dioxide Capture Using Amine-Functionalized Multiwalled Carbon Nanotubes. *Energy Fuels* **2014**, *28*, 6494−6501.

(49) Fan, Y.; Labreche, Y.; Lively, R. P.; Jones, C. W.; Koros, W. J. Dynamic CO$_2$ Adsorption Performance of Internally Cooled Silica-Supported Poly(ethylenimine) Hollow Fiber Sorbents. *AIChE J.* **2014**, *60*, 3878−3887.

(50) Yu, K.; Kiesling, K.; Schmidt, J. R. Trace Flue Gas Contaminants Poison Coordinatively Unsaturated Metal−Organic Frameworks: Implications for CO$_2$ Adsorption and Separation. *J. Phys. Chem. C* **2012**, *116*, 20480−20488.

(51) Sanz-Pérez, E. S.; Olivares-Marín, M.; Arencibia, A.; Sanz, R.; Calleja, G.; Maroto-Valer, M. M. CO$_2$ Adsorption Performance of Amino-Functionalized SBA-15 Under Post-Combustion Conditions. *Int. J. Greenhouse Gas Control* **2013**, *17*, 366−375.

(52) Pekov, I. V.; Chukanov, N. V.; Britvin, S. N.; Kabalov, Y. K.; Göttlicher, J.; Yapaskurt, V. O.; Zadov, A. E.; Krivovichev, S. V.; Schüller, W.; Ternes, B. The Sulfite Anion in Ettringite-Group Minerals: A New Mineral Species Hielscherite, Ca$_3$Si(OH)$_6$(SO$_4$)-(SO$_3$)●11H$_2$O, and the Thaumasite−Hielscherite Solid-Solution Series. *Mineral. Mag.* **2012**, *76*, 1133−1152.

(53) Wang, C.; Cui, G.; Luo, X.; Xu, Y.; Li, H.; Dai, S. Highly Efficient and Reversible SO$_2$ Capture by Tunable Azole-Based Ionic Liquids Through Multiple-Site Chemical Absorption. *J. Am. Chem. Soc.* **2011**, *133*, 11916−11919.

(54) Hungerford, J.; Bhattacharyya, S.; Tumuluri, U.; Nair, S.; Wu, Z.; Walton, K. S. DMOF-1 as a Representative MOF for SO$_2$ Adsorption in Both Humid and Dry Conditions. *J. Phys. Chem. C* **2018**, *122*, 23493−23500.

(55) Lee, H. J.; Lee, K. I.; Kim, M.; Suh, Y. W.; Kim, H. S.; Lee, H. Diamine-Anchored Polystyrene Resins for Reversible SO$_2$ Adsorption. *ACS Sustainable Chem. Eng.* **2016**, *4*, 2012−2019.

(56) Colthup, N.; Daly, L.; Wiberley, S. *Introduction to Infrared and Raman Spectroscopy*, 2nd ed.; Academic Press, 1975.

(57) Miller, F. A.; Wilkins, C. H. Infrared Spectra and Characteristic Frequencies of Inorganic Ions. *Anal. Chem.* **1952**, *24*, 1253−1294.

(58) Xu, J.; Liu, Y. M.; Lipton, A. S.; Ye, J.; Hoatson, G. L.; Milner, P. J.; McDonald, T. M.; Siegelman, R. L.; Forse, A. C.; Smit, B.; Long, J. R.; Reimer, J. A. Amine Dynamics in Diamine-Appended Mg$_2$(dobpdc) Metal−Organic Frameworks. *J. Phys. Chem. Lett.* **2019**, *10*, 7044−7049.

(59) Lee, J.-H.; Siegelman, R. L.; Maserati, L.; Rangel, T.; Helms, B. A.; Long, J. R.; Neaton, J. B. Enhancement of CO$_2$ Binding and Mechanical Properties upon Diamine Functionalization of M$_2$(dobpdc) Metal−Organic Frameworks. *Chem. Sci.* **2018**, *9*, 5197−5206.

(60) Tailor, R.; Abboud, M.; Sayari, A. Supported Polytertiary Amines: Highly Efficient and Selective SO$_2$ Adsorbents. *Environ. Sci. Technol.* **2014**, *48*, 2025−2034.

(61) Tailor, R.; Ahmadalinezhad, A.; Sayari, A. Selective Removal of SO_2 Over Tertiary Amine-Containing Materials. *Chem. Eng. J.* **2014**, *240*, 462−468.

(62) Barker, D. A.; Turner, S. A.; Napier-Moore, P. A.; Clark, M.; Davison, J. E. CO_2 Capture in the Cement Industry. *Energy Procedia* **2009**, *1*, 87−94.

(63) Holmes, H. E.; Lively, R. P.; Realff, M. J. Defining Targets for Adsorbent Material Performance to Enable Viable BECCS Processes. *JACS Au* **2021**, *1*, 795−806.